Title

A lithium-sulfur battery with a solution-mediated pathway operating under lean electrolyte conditions

Authors

Wang, Hui
Shao, Yuyan
Pan, Huilin
et al.

Publication Date

2020-10-01

DOI

10.1016/j.nanoen.2020.105041

Peer reviewed

A lithium-sulfur battery with a solution-mediated pathway operating under lean electrolyte conditions

Hui Wang[1,2], Yuyan Shao[1,2], Huilin Pan[1,2], Xuefei Feng[3], Ying Chen[1,4], Yi-Sheng Liu[3], Eric D Walter[4], Mark H. Engelhard[5], Kee Sung Han[1,4], Tao Deng[2], Guoxi Ren[3], Dongping Lu[2], Xiaochuan Lu[2], Wu Xu[2], Chunsheng Wang[6], Jun Feng[3], Karl T. Mueller[1,4], Jinghua Guo[3], Kevin R. Zavadil[6], and Ji-Guang Zhang[1,2*]

1. Joint Center for Energy Storage Research (JCESR), Pacific Northwest National Laboratory, Richland, WA 99354, USA
2. Energy & Environment Directorate, Pacific Northwest National Laboratory, Richland, Washington 99354, USA
3. Advanced Light Source, Lawrence Berkeley National Laboratory, Berkeley, CA 94720, USA.
4. Physical and Computational Sciences Directorate, Pacific Northwest National Laboratory, Richland, Washington 99354, USA
5. Environmental Molecular Sciences Laboratory, Pacific Northwest National Laboratory, Richland, Washington 99354, USA
6. Joint Center for Energy Storage Research (JCESR), Sandia National Laboratories, PO BOX 5800, Albuquerque, New Mexico 87185, USA.

Corresponding author: J.-G. Zhang, jiguang.zhang@pnnl.gov

Abstract

Lithium-sulfur (Li-S) battery is one of the most promising candidates for the next generation energy storage systems. However, several barriers, including polysulfide shuttle effect, the slow solid-solid surface reaction pathway in the lower discharge plateau, and corrosion of Li anode still limit its practical applications, especially under the lean electrolyte condition required for high energy density. Here, we propose a solution-mediated sulfur reduction pathway to improve the capacity and reversibility of the sulfur cathode and suppress dendrite growth on the Li metal anode simultaneously. With this method, a high coulombic efficiency (99%) and stable cycle life over 100 cycles were achieved under application-relevant conditions (S loading: 6.2 mg cm^{-2}; electrolyte to sulfur ratio: 3 mL_E g_s^{-1}; sulfur weight ratio: 72 wt%). This result is enabled by a specially designed Li_2S_4-rich electrolyte, in which Li_2S is formed through a chemical disproportionation reaction instead of electrochemical routes. A diglyme solvent was used to obtain electrolytes with the optimum range of Li_2S_4 concentration. Operando X-ray absorption spectroscopy confirms the solution pathway in a practical Li-S cell. This solution pathway not only introduces a new electrolyte regime for practical Li-S batteries, but also provides a new perspective for bypassing the inefficient surface pathway for other electrochemical processes.

Introduction

The development of rechargeable lithium-sulfur (Li-S) batteries based on conversions reaction is driven by their higher theoretical specific energy at reduced cost compared to those of Li-ion batteries based on intercalation reactions[1-6]. However, Li-S batteries still suffer from their limited cycle life and low specific energy under flooded electrolyte conditions. These challenges are related to the continuous irreversible passivation of electrode by insulation Li_2S and the deteriorating solid-electrolyte interphases on the Li metal anode upon cycling under high sulfur loadings[7-9]. To overcome these challenges and reach the full potentials of Li-S chemistry, it is essential to tune electrolyte formulations to enable a robust interface and a new reversible pathway for Li-S reactions[10-15].

Full sulfur-utilization has rarely been reported in solvent-flooded Li-S cells, where the traditional binary ether solvent of 1,3-dioxolane (DOL) and 1,2-dimethoxyethane (DME) are used[16, 17]. Most of the reported specific capacity of sulfur cathode is less than 1200 mAh g^{-1} (i.e., 71.6 % of sulfur utilization based on its theoretical capacity of 1672 mAh g^{-1}), limited by a surface pathway in the lower discharge plateau because the active surface area is decreasing during discharge[18]. Recently, a new strategy of sparingly solvating electrolytes has been proposed to render a significant increase in the sulfur utilization at elevated temperature owing to the increased concentration of $S_3^{\cdot-}$ radical in a high dielectric constant (DC) solvent of acetonitrile, where a chemical/electrochemical redox pathway involving $S_3^{\cdot-}$ was proposed to take place simultaneously [19, 20]. In other words, the full sulfur utilization enabled by this pathway strongly relies on the concentration of $S_3^{\cdot-}$ [21, 22]. However, the poor compatibility of high DC solvents against Li metal has been an unsettled hurdle and the aggressive nucleophilic attack of DOL and carbonate solvents by $S_3^{\cdot-}$ has been extensively studied[23-25]. Fortunately, the Li-benign linear ether solvents, except for DME, have been experimentally confirmed to be resistant to $S_3^{\cdot-}$ attack[26, 27]. Linear ethers with a higher number of solvating oxygen atoms are found to enhance the stability of the solvent-Li^+ solvating complex and thus the stability of $S_3^{\cdot-}$.

Li salts with different anions have been reported to greatly affect the solubility of low-order Li polysulfides (LiPS) and thus the concentration of $S_3^{\cdot-}$, since the latter is a product of the disproportionation reaction equilibrium of LiPS[28, 29]. Higher ionic-association-strength (i.e., high Lewis basicity) of anion X^- ($X^- = NO_3^-$, $CF_3SO_3^-$, Br^-, etc.) has been demonstrated to render a higher concentration of low-order LiPS due to a stronger interaction between Li^+ from LiPS and X^-, compared to the low ionic-association-strength of the base anion of $N(CF_3SO_2)_2^-$ (bis(trifluoromethanesulfonyl)imide [$TFSI^-$]). One can thus expect that tuning electrolyte formulations, especially through highly solvating Li-benign linear ether solvents [10] and high ionic-association-strength anions, can steer a synergetic chemical/electrochemical sulfur redox pathway in the lower discharge plateau by the presence of stabilized $S_3^{\cdot-}$.

In this work, we report a solution-mediated chemical/electrochemical sulfur redox pathway, enabled by the optimal Li_2S_4 concentration in the electrolyte, to circumvent undesired solid charge-transfer process. We demonstrated that this new approach can boost the sulfur utilization and cyclability of Li-S batteries with high sulfur loadings (> 6 mg cm^{-2}) under lean

electrolyte conditions at room temperature. In particular, diglyme (G2) is employed to prepare an optimized high concentration of Li_2S_4 with the aid of NO_3^-. This Li_2S_4-retaining strategy is feasible to decouple the sulfur reduction pathway from both the bulk electrolyte and the electroactive surface area, to circumvent conventional solid-solid charge transfer in the lower discharge plateau, and to make reversible Li stripping/plating.

Results and discussion

A new Li_2S_4-dictated pathway under lean electrolyte conditions

In a Li-S cell with a critical electrolyte-to-sulfur (E/S) ratio (i.e., ≤ 4.0 mL_E g_s^{-1} when the maximum solubility of LiPS reaches 8 M [S]; where mL_E and g_s represent volume of electrolyte and weight of sulfur in Li-S cell, respectively, **Supplementary Fig. 1**), sulfur is first reduced at the cathode during discharge to form quasi-solid Li_2S_4 by reactions [1-2] as shown below [30]. In the subsequent reaction represented by the lower discharge plateau [3], nucleation and growth barriers of insulating solid Li_2S present a tremendous hurdle for Li^+ diffusion and solid-solid charge-transfer process.

$$S_8\ (s) + 2Li^+ + 2e^- \rightarrow Li_2S_8\ (s \text{ or } l) \qquad [1]$$

$$Li_2S_8\ (s \text{ or } l) + 2Li^+ + 2e^- \rightarrow 2Li_2S_4\ (s) \qquad [2]$$

$$Li_2S_4\ (s) + 6Li^+ + 6e^- \rightarrow 4\ Li_2S\ (s) \qquad [3];\ E^{\Theta}=2.1\ V$$

In order to investigate electrolyte dependence of sulfur utilization in the lower discharge plateau under lean electrolyte conditions, selection of a carbonaceous model matrix is important to eliminate effects of the diffusion/migration of high-order LiPS in the bulk electrolytes from cathodes. A microporous sulfur-loading matrix of activated carbon fiber cloth (ACFC) was used as a model substrate (**Supplementary Fig. 2**) because it can confine high-order LiPS in micropores.[11] Despite different electrolytes and sulfur sources, no diffusion/migration of high-order LiPS from micropores of ACFC was observed in cyclic voltammograms (**Supplementary Fig. 2**). Moreover, the relatively high pore volume of ACFC allows high sulfur loadings in micropores with limited solvent permeation [11], akin to where the Li-S redox reactions would take place in practical applications.

A Li-S cell was assembled with a sulfur containing electrolyte E_G2_0.5 M Li_2S_4 (E_G2 represents 1 M LiTFSI_0.3 M $LiNO_3$ in G2) as the sulfur source and ACFC as the carbon matrix. Sulfur loading is 1.58 mg cm^{-2} calculated by total amount of sulfur in the electrolyte divided by the area of ACFC electrode. A typical discharge/charge curve is shown in **Fig. 1a**, which shows a discharge capacity of 1590 mAh g_s^{-1} and a coulombic efficiency (CE) of 99.1 %, suggesting that 95.1 % of the sulfur is reduced to solid Li_2S. To determine the sulfur reduction mechanism in E_G2_0.5 M Li_2S_4, potentiodynamic cycling with galvanostatic acceleration (PCGA) was performed in the Li|E_G2_0.5 M Li_2S_4|ACFC; results are shown in **Fig. 1b**. PCGA is a quasi-equilibrium technique that can provide very useful detailed information on electrochemical

processes by analyzing the integral of the current during the step time (δQ) versus the potential in the same step. The reversibility of solid Li_2S_4 reduction at 2.06 V and oxidation at 2.22 V is high, as indicated by the observed comparable δQs and the narrow potential difference of 0.16 V between the two reactions, which further supports ACFC as a model material. Interestingly, there is an additional broad reduction peak below the major reduction. To unravel the origin of the broad reduction peak in the 1.98-1.99 V, the dependence of PCGA traces for the discharge of Li-S cell on Li_2S_4 concentrations and stepwise potentials was then investigated and the results are shown in **Supplementary Fig. 3.** No broad reduction peak was observed for the cell without Li_2S_4 (E_G2), indicating the strong dependence on the electroactive species of Li_2S_4 of this broad reduction peak in **Supplementary Fig. 3a.** Prior to this broad peak, a major sharp reduction peak, corresponding to the major electrochemical reduction of Li_2S_4 from bulk electrolyte, is observed and increases with increasing concentration of Li_2S_4. However, the following broad reduction peak is inversely weakened, which is also in line with the stepwise potential dependence of PCGA measurement results using the same cell in **Supplementary Fig. 3b**. The size of this broad reduction peak is thus closely related to the Li_2S_4-retaining in the bulk electrolytes, suggesting a new reduction pathway for sulfur in micropores.

The cell using E_G2_0.5 M Li_2S_4 was cycled at the much lower rate of 0.075C; results are shown in **Fig. 1c**. A gradual increase in the discharge capacity was observed in the initial cycles probably due to the improved wetting ability of ACFC[31, 32]. After the 10th cycle, both the maximum deliverable discharge capacity (i.e. 1590 mAh g_s^{-1}) and CE of the cell continuously decay upon further cycling, suggesting the sulfur redox environment significantly evolves within ACFC as soon as most sulfur from Li_2S_4 in bulk electrolytes migrates into ACFC and only sparse Li_2S_4 is remained outside ACFC. An identical cell discharged at 0.3 C showed an increasing discharge capacity from 825 to 979 mAh g_s^{-1} and an ultrahigh average CE of 99.7 % for 100 cycles (**Fig. 1c**). During fast discharges, appropriately half of the Li_2S_4 (i.e., 0.25 M) remained outside the ACFC, assuming 100 % sulfur utilization in micropores (**Fig. 1a**) at the delivered specific capacity of 836 mAh g_s^{-1}. Further, a new cell with E'_G2_1.5 M Li_2S_4 (E'_G2: 1 M LiTFSI_0.9 M $LiNO_3$ in G2) was deliberately discharged at 0.075C, as shown in **Fig. 1d**. This cell delivered a relatively high specific capacity of *ca.*1200 mAh g_s^{-1} and an average CE as high as 99.8 %, compared to 96.9 % for the cell using 0.5 M Li_2S_4. The Li_2S_4 remaining at the outside of ACFC is estimated to be 0.42 M in this cell during cycling. These results clearly suggest that Li_2S_4 remaining on the outside of the ACFC plays a special role in enabling a high sulfur utilization in the lower discharge plateau with limited solvents permeation (i.e. lean electrolyte conditions).

We also compared the effect of different sulfur species loaded by different approaches on the performance of Li-S cells, with the same total sulfur loading (including those in electrode and electrolyte) and electrolytes volume. Three Li-S cells using ACFC were prepared as shown in **Supplementary Fig. 4**. In the **Supplementary Fig. 4a-b**, sulfur was introduced into ACFC prior to cell assembly (see Method section for details). In the **Supplementary Fig. 4c**, no sulfur presents in ACFC prior to cell assembly and all the sulfur in the cell originate from electrolyte. The electrolytes used in these three cells are base electrolyte-E_DOL/DME: 1 M LiTFSI_0.30 M

$LiNO_3$ in DOL/DME (**Supplementary Fig. 4**b), E_G2 (**Supplementary Fig. 4**a), and E_G2_0.5 M Li_2S_4 (**Supplementary Fig. 4**c). All cells were tested at 0.3 C rate and 30 °C. After 500 cycles, the lower discharge plateau corresponding to reaction [3] totally disappeared and the capacity decay was almost continuous in the cells using E_G2 and E_DOL/DME, suggesting the surface pathway of reaction [3] should prevail in these two cells to result in a parasitic loss of surface area by the passivation of Li_2S during cycling. However, the length of the lower discharge plateau has a minimal change for the cell using E_G2_0.5 M Li_2S_4. This indicates that the presence of excess Li_2S_4 in the electrolyte is helpful to stabilize the lower discharge plateau during cycling.

Dependence of sulfur utilization efficiency on the content of Li_2S_4 in electrolyte

To further correlate the interplay between Li_2S_4 content in the bulk electrolyte and the reduction efficiency of solid Li_2S_4 under lean electrolyte conditions, ACFC_Li_2S_8 was prepared by preloading 30 μL of 1 M Li_2S_8 (sulfur mass loading: 6.06 mg cm^{-2}) into ACFC. **Fig. 2a** shows typical discharge curves of Li | E_G2_*x* M Li_2S_4 | ACFC_1 M Li_2S_8 with an E/S ratio of 3.0 mL_E $g_{s\_cathode}^{-1}$ at 0.12 mA cm^{-2} and 30 °C, where $g_{s\_cathode}$ represents the weight of sulfur in cathode (not including those in electrolyte). The achievable discharge capacity shows a strong correlation with the concentration of Li_2S_4 in the electrolyte. The cell using E_G2_0.5 M Li_2S_4 shows a significantly high capacity of 1520 mAh $g_{s\_cathode}^{-1}$ based on preloaded Li_2S_8 and1268 mA $g_{s\_total}^{-1}$ based on the total sulfur loading (including those pre-loaded in ACFC and those in the electrolyte) at an elevated discharge potential. In contrast, limited capacities of < 400 mAh $g_{s\_cathode}^{-1}$ were observed for lower (<0.5 M) and higher concentrations (0.75 M) of Li_2S_4, indicating that an optimal concentration of Li_2S_4 in the bulk electrolytes is required to reduce preloaded Li_2S_8 to solid Li_2S_4 and the following Li_2S effectively. This is the first time that nearly 100% solid Li_2S_4 reduction has been reported for Li-S coin cells with high sulfur loadings and lean electrolytes.

Cells were both halted near the nucleation stage using the couple of E_G2|ACFC_Li_2S_8 or E_G2_0.50 M Li_2S_4|ACFC_S_8 in the **Fig. 2b** and **Supplementary Fig. 5** indicate that both the starting sulfur material and the 0.5 M Li_2S_4 content in electrolyte have a remarkable impact on the sulfur utilization. The cell using E_DOL/DME presents a lower discharge plateau, at 1.85 V, and a limited discharge capacity of 897 mAh $g_{s\_cathode}^{-1}$, far below that of the cell using E_G2_0.50 M Li_2S_4. Moreover, bulk electrolytes with 2 M [S] were made from 0.25 M Li_2S_8 and 0.33 M Li_2S_6 and examined, as shown in **Fig. 2c**. Interestingly, the cell using 0.33 M Li_2S_6 shows the absence of a lower discharge plateau. However, the cell using 0.25 M Li_2S_8 presents a specific capacity of 1884 mAh $g_{s\_cathode}^{-1}$, indicating that sulfur from the bulk electrolyte of 0.25 M Li_2S_8 migrated into the ACFC and contributed to the total capacity due to the concurrent reduction of Li_2S_8 from the bulk electrolyte and the ACFC, where the intermediate reduced species of Li_2S_6 are not supposed to generate from E_G2_0.25 M Li_2S_8; otherwise, it would exhibit no lower discharge plateau, as did the cell using E_G2_0.33 M Li_2S_6.

Fig. 2d shows the discharge PCGA traces obtained from cells using E_DOL/DME and E_G2_0.50 M Li_2S_4. The PCGA trace of the cell using E_G2_0.50 M Li_2S_4 presented another unusual sulfur reduction pathway, where multiple discharge reactions are shown to take place at 2.09, 1.95, 1.90, and 1.85 V, respectively. It shows a continuously increasing incremental charge upon cathodic sweeping, with the maximum observed at 1.85 V. However, for the cell using E_DOL/DME, only two peaks were observed, at 2.13 V and 1.83 V, with a decreasing incremental charge upon cathodic sweeping, which further corroborates that Li_2S_4 retention can significantly affect the reduction pathway of sulfur species from high sulfur loadings under lean electrolyte conditions.

A solution-mediated chemical/electrochemical route

To explain the strong correlation between Li_2S_4 content in electrolyte and the ultrahigh sulfur utilization under lean electrolyte conditions, we propose a solution pathway enabled by Li_2S_4-mediated reaction (**Fig. 3a**) to divide reaction [3] into the following steps:

At the potential dip (i.e., the onset of nucleation of Li_2S):

$$3S_4^{2-}\,(l) \Leftrightarrow 2\,S_3^{\cdot-} + 2S_3^{2-}\,(l) \qquad [4]$$

$$2S_3^{\cdot-} + 2e^- \rightarrow 2S_3^{2-}\,(l) \qquad [5]$$

After the potential dip in the elevated discharge plateau:

$$S_3^{2-}\,(l) + Li_2S_4\,(s) \Leftrightarrow Li_2S\,(s) + S_6^{2-}\,(l) \qquad [6]$$

$$S_6^{2-}\,(l) + 2e^- \rightarrow 2S_3^{2-}\,(l) \qquad [7],\ E^{\Theta}=2.3\ V$$

The presence of optimal-concentration Li_2S_4 in the bulk electrolyte drives the chemical disproportionation reaction [4] toward $S_3^{\cdot-}$, which is further reduced to soluble S_3^{2-} by reaction [5] [22, 26]. Reactions [4] and [5] have been investigated by *in-situ* ultraviolet-visible absorption spectroscopy and electron paramagnetic resonance (EPR) spectroscopy in a tetraglyme-based electrolyte [18, 26]. The soluble S_3^{2-} from reaction [5] chemically reacts with quasi-solid Li_2S_4 (reaction [6]) and generate Li_2S precipitate and soluble S_6^{2-}; the soluble and replenishable S_6^{2-} is further reduced into soluble S_3^{2-} (reaction [7]) at a higher redox potential (i.e. $E^{\Theta}=2.3$ V) [21] than reaction [3] (i.e. $E^{\Theta}=2.1$ V) [31] and [5], which prevents further reduction of bulk Li_2S_4 on cathodes and result in the voltage dip before the onset of the lower discharge plateau. The reduction efficiency of solid Li_2S_4 is thus not affected by the decreasing available surface area during single discharge, and could potentially reach 100% by reactions [6] and [7]. **Fig. 2a** shows that the optimal concentration of Li_2S_4, that can allow reactions [4] to [7] (i.e., the synergetic chemical/electrochemical reactions) to take place with a low energy barrier and an elevated discharge plateau, is 0.50 M (i.e., optimal concentration ratio of S_3^{2-}/ S_6^{2-}). The solubility of

Li_2S_4 was reported to be as low as 0.0625 M in DOL/DME.[28]The low solubility of Li_2S_4 and the poor stability of S_3^{*-} in DME and DOL (i.e., low concentration ratio of S_3^{2-}/ S_6^{2-}) [24, 27] means the synergetic chemical/electrochemical reactions are not likely to take place in the DOL/DME-based electrolytes. This is evidenced by the lack of elevation of the lower discharge plateau and a much lower discharge specific capacity, as shown in **Fig. 2b**. Reaction [6] will not take place in a low concentration ratio of S_3^{2-}/S_6^{2-} (CS_3^{2-}/CS_6^{2-}) if the bulk electrolytes still contain S_6^{2-} when the cell discharges beyond reaction [2], as depicted in **Fig. 3b and demonstrated in Fig. 2c**, and if the bulk electrolytes contains low concentration of CS_3^{2-} originating from low concentration of CS_4^{2-} **in Fig. 2a.** Further, a higher concentration of Li_2S_4 is found to result in a substantial decrease of lithium cation diffusion coefficient by ^{7}Li PFG-NMR measurements (**Supplementary Table 1**) to maintain the charge neutrality and then decrease the local supply of S_3^{2-}.

To investigate the solvent-dependent of $S_3^{\cdot-}$ in electrolytes, non-invasive EPR measurements were performed for electrolytes of E_G2, E_G2_0.5 M Li_2S_4 and E_DOL/DME_saturated Li_2S_4 (images shown in **Supplementary Fig. 6**) in **Fig. 3c**. EPR spectrum at 125 K of E_G2_0.5 M Li_2S_4 clearly reveals the pattern of $S_3^{\cdot-}$ radical at g=2.034[15, 18], and the EPR spectrum also shows the persistent presence of the radical at room temperature (T=298 K). Similar pattern was not observed for E_G2 and greatly weakened for E_DOL/DME_saturated Li_2S_4. The concentration of $S_3^{\cdot-}$ radical is calculated to be 0, 0.6 mM, and 11.2 mM for E_G2, E_DOL/DME_saturated Li_2S_4 and E_G2_0.5 M Li_2S_4 respectively; the large difference in the concentration of $S_3^{\cdot-}$ clearly highlights the dramatic impact of solvents on the presence of $S_3^{\cdot-}$ and the resultant CS_3^{2-} that steers distinctive sulfur reduction pathway. Raman results further confirm the presence of $S_3^{\cdot-}$ in E_G2_0.5 M Li_2S_4 as shown in **Supplementary Fig. 7**, where a dominant and sharp peak of 534.6 cm^{-1} stemming from $S_3^{\cdot-}$ was observed [34].

Experimental verification of the Li_2S_4-enabled solution pathway

Since Li_2S_4 retention in the bulk electrolyte can drastically enhance the sulfur utilization under lean electrolyte conditions, it is very important to directly demonstrate whether or not Li_2S_4 plays a role in the proposed solution pathway. To demonstrate the occurrence of synergetic chemical/electrochemical reactions, operando sulfur K-edge X-ray absorption spectroscopy (XAS) was employed to probe sulfur speciation in a Li-S cell using electrospun carbon fiber (ECF) and Li_2S_8, with E_G2_0.5 M Li_2S_4 as the bulk electrolyte.

Identification of $S_3^{\cdot-}$ (i.e. a kick-off agent of reaction [6]) through XAS can be used as a criteria for verification of Li_2S_4-enabled solution pathway. Based on the above discussions, strong $S_3^{\cdot-}$ signal should only occur in a Li-S cell using E_G2 and E_G2_0.5 M Li_2S_4 electrolyte, not in a Li-S cell with no pre-added Li_2S_4 electrolyte (such as E_G2). This means the occurrence of $S_3^{\cdot-}$ depends on the composition of electrolytes, not on the selection of carbon host. Considering the very week signal obtained in our initial experiment when ACFC host is used, we replaced ACFC by ECF in the final experiment because the cells with ECF host is much thinner than ACFC host (with the similar capacity) and exhibit a much stronger XAS signal for $S_3^{\cdot-}$. Fingerprints of Li_2S_4, Li_2S_3, Li_2S_6, and Li_2S reported in previous articles are summarized in

Supplementary Table 2[27, 35, 36]. Although it is nontrivial to experimentally prepare individual LiPS specimen for enriching the XAS reference data pool, the simulated fingerprint peaks computed from the advanced simulation method considering the impact of solvent (e.g. the ethereal solvent of tetraglyme) can allow us to make a distinct interpretation of XAS spectra, since preparing a single LiPS is impeded by the occurring of LiPS disproportionation reaction in a low concentration at low temperatures[37].

Fig. 4a-b show XAS contours collected from Li-S cells using E_G2 and E_G2_0.5 M Li_2S_4 at ambient temperature, respectively, and the corresponding operando discharge curves of XAS Li-S cells. Assignment of each LiPS is based on **Supplementary Table 2**. Each LiPS possesses a main peak and pre-edge peak with a relative intensity ratio (i.e. the color difference). **Fig.4a** shows a normal XAS evolution with continuously color change from Li_2S_8 (i.e. the continuously decaying of the color for the main peak of 2472.6 eV for Li_2S_8) upon the initial discharge (0-148 mAh $g_{s\_cathode}^{-1}$). However, there is no continuous intensified/fading X-ray absorbance was observed in **Fig. 4b** for an individual LiPS. In theory, electrochemically reduced Li_2S cannot be observed until the discharge capacity reaches 209 mAh $g_{s\_cathode}^{-1}$ based on the preloaded Li_2S_8. However, the major characteristic peaks for Li_2S_6 (2472.7 eV) and Li_2S (2474.2 eV) intensified or diminished in synchrony during the discharge of 57–179 mAh $g_{S\_cathode}^{-1}$, which is further evidenced by the emergence of "valley plain" in 2474-2477 eV of individual XAS spectrum (e.g. 161 mAh $g_{s\_cathode}^{-1}$) due to the opposite intensity evolution of LiPS and Li_2S in this experimental and computed energy range as shown in **Supplementary Fig. 8.** No valley plain was observed for cells using E_G2 in the whole XAS spectra, indicating no Li_2S was generated in the initial discharge for this cell. The presence of valley plain can be regarded as an evidence of the occurrence of chemical reaction [6]. Although the intensity of $S_3^{\cdot-}$ (i.e. a kick-off agent of reaction [6]) is relatively small compared to those of other LiPS, the evolution of $S_3^{\cdot-}$ at 2468.5 eV is still distinguishable in **Fig. 4b.** It is interesting to note that the abrupt drop of cell voltage at 127 mAh $g_{S\_cathode}^{-1}$ of the discharge curve for operando XAS cell using E_G2_0.5 M Li_2S_4 (Fig. 4b) coincides with the transient intensity reduction of LiPSs including $S_3^{\cdot-}$ observed in a similar XAS cell used in Fig. 4b, after which the cell voltage recovers rapidly to a higher voltage plateau due to reactions [6] and [7] [21] and avoids the premature termination of discharge. The corresponding intensity of LiPSs including $S_3^{\cdot-}$ also recovers after this point. The special fingerprint peak of $S_3^{\cdot-}$ is observed to show the maximum intensity at 160 mAh $g_{s\_cathode}^{-1}$ in Fig. 4b. The increased intensity of $S_3^{\cdot-}$ is only originate from the disproportionation reaction (S_6^{2-} -- $2S_3^{\cdot-}$) of Li_2S_6. Generation of Li_2S_6 can be further evidenced by the intensity evolution of $S_3^{\cdot-}$. **Fig. 4c-d** display the pile-up of individual XAS spectrum every 40 mAh $g_{s\_cathode}^{-1}$ for cells using E_G2 and E_G2_0.5 M Li_2S_4, respectively. An isosbestic-related point [38] at 2478.8 eV was surprisingly found for cell using E_G2_0.5 M Li_2S_4 but not for cell using E_G2. These operando XAS spectra clearly demonstrate that Li_2S can be chemically produced, along with Li_2S_6, by synergetic chemical/electrochemical reactions before the onset of electrochemical reduction of solid Li_2S_4 through the surface pathway.

In a parallel experiment using the XAS cell of Li|E_G2_0.5 M Li_2S_4| ECF_Li_2S_8 (sulfur loading: >6 mg $cm^{-2;}$ $E/S_{cathode}$ ratio: 3.0), the final solid discharge product was harvested when the cell was terminated discharging at 1431 mAh $g_{s\_cathode}^{-1}$ (full discharge) to characterize its composition by ex-situ X-ray photoelectron spectroscopy (XPS) measurement as shown in

Supplementary Fig. 9a. The dominant final solid product can be determined as Li_2S by corresponding fitted peaks of S_{2p}[37, 38] as shown in **Supplementary Fig. 9b** and quantitative calculation with an accuracy of 96.5 % in **Supplementary Table 3.**

Application of the Li_2S_4-enabled solution pathway

In this work, advantages of Li_2S_4 content in bulk electrolytes have been demonstrated (**Fig. 1d** and **Supplementary Fig. 4**), in terms of steering the synergetic chemical/electrochemical reactions (**Fig. 4**) and high compatibility with Li metal (discussed in the Supplementary Notes and shown in **Supplementary Figs. 10–14.** Li-S cells with high sulfur loadings and under lean electrolyte conditions are expected to deliver a high specific capacity and long cycle life if the cell were just cycled between Li_2S_4 and Li_2S, with a theoretical capacity of 1254 mAh g_s^{-1}, by the Li_2S_4-retaining solution pathway.

ACFC was initially used as a model material to study the electrolyte-dependent sulfur reduction pathway under lean electrolyte conditions. Surprisingly, even Li-S cells using ACFC are fully charged at 2.8 V, where the retained Li_2S_4 might be oxidized into Li_2S_8 or migrate toward the Li metal anode with Li^+ owing to the stronger interaction between Li^+ and short-order LiPS[41], high sulfur utilization and CE are still maintained as observed in **Fig. 1**. This indicates that Li_2S_4, not the intermediate Li_2S_6, is always generated from the reduction of Li_2S_8 in G2 to continuously prevail as the solution pathway in ACFC. **Supplementary Figs. 15** shows the cycling performance of Li|E'_G2_1.5 M Li_2S_4|ACFC with a high sulfur loading of 7.6 mg cm^{-2} at 1/30C (i.e., 0.42 mA cm^{-2}) for discharging, and 1/7.5C for charging in the range 1.80–2.80 V. The E/S ratio was determined to be 5.20. The potential dip is greatly alleviated, even though the cell was charged to 2.8 V. Moreover, both excellent cycling retention and high CE can be achieved with a stable areal capacity of *ca.* 6 mAh cm^{-2}. Impact of the charge cut-off potential of Li|E'_G2_1.5 M Li_2S_4|ACFC on the middle discharge potential (i.e. an indication of cell cycling retention and the sustainability of solution-mediated pathway) was investigated for 20 cycles with the same charge/discharge rate of 1/30 C at 30 °C as shown in Supplementary Fig. 16. Two different charge cut-off potentials of 2.63 V (i.e. oxidation to Li_2S_8) and 2.48 V (i.e. roughly oxidation to Li_2S_4) were selected based on CV measurement of this cell (Supplementary Fig. 16a). The cell terminated at 2.48 V showed a stable middle discharge potential but the cell terminated at 2.63 V showed a rapid decrease in the middle discharge potential, indicating the solution pathway is highly sustained when the charge cut-off potential is carefully tuned to terminate the cell charge to the stage of Li_2S_4.

To demonstrate the general application of the Li_2S_4-enabled solution pathway, Electrospun carbon fiber (ECF) has been used to replace ACFC as sulfur-loading substrate because ECF is a typical macroporous carbon matrix which cannot prevent diffusion of high-order LiPS (i.e., soluble S_6^{2-} in reaction [6]) into electrolytes, and thus can be used to verify the Li_2S_4-enabled solution pathway. The Li| E_G2_0.5 M Li_2S_4|ECF_Li_2S_8 cell was cycled with a high sulfur loading of 6.2 mg cm^{-2} at an $E/S_{cathode}$ ratio of 3.0, 0.20 mA cm^{-2}, and 30 °C in the range 1.80–2.45 V, as shown in **Fig. 5**. The low charge cutoff potential of 2.45 V was deliberately chosen to prevent the oxidation of high-order LiPS into S_8 on the ECF and the

migration of high-order LiPS toward Li (**Supplementary Fig. 17**) [42]. The Li-S cell shows potential-vs.-capacity curves resembling those of the Li|E_G2_0.5 M Li_2S_4|ACFC_Li_2S_8 cell (**Fig. 2**). The presence of Li_2S_4 can be signified by the continuous potential dip at approximately 50 mAh $g_{s\_cathode}^{-1}$ and by the high average CE of 99.0 % upon cycling. It is thus reasonable to postulate that the Li_2S_4-enabled solution pathway prevails in this Li-S cell. The initial discharge capacity is lower than that observed using ACFC, probably due to the capacity loss from uncontrollable diffusion of S_6^{2-}. After 100 cycles, the cell can sustain the lower discharge plateau and deliver a specific capacity as high as 518 mAh g^{-1} based on Li_2S_8 preloaded in ECF cathode and 328 mAh g^{-1} based on the total sulfur from cathode and 0.5 M Li_2S_4 in electrolyte. Very few Li-S coin cells have been reported so far to survive for more than 40 cycles, with the continuous presence of the discharge plateau under similar conditions.[43] The kinetics of the Li-S cell can be further improved by incorporation of a smart material (i.e., possessing high electronic conductivity and high Li^+ transport) into the carbon matrix under lean electrolyte conditions.[44]

In summary, a solution-mediated pathway for sulfur reduction embracing synergetic chemical and electrochemical processes is described in Li-S cells with high sulfur loadings under lean electrolyte conditions. Excellent cycling performance of prototype Li-S cells validates the feasibility of developing practical Li-S cells using the Li_2S_4-retaining strategy.

Data availability. Data supporting the finds of this study are available within the paper and its Supplementary Information file, and are available from the corresponding author upon reasonable request.

Acknowledgements

This work was supported as part of the Joint Center for Energy Storage Research, an Energy Innovation Hub funded by the U.S. Department of Energy (DOE), Office of Science, Basic Energy Sciences. Authors thank Dr. Nathan Canfield and Dr. Haiping Jia for SEM characterizations., Dr. Xiaolin Li for help on electrospinning setup, and Dr. Patrick Z El Khoury for help on Raman characterization. ACFC samples were kindly supplied by the Carbon Materials Division of Kuraray Co., Ltd, Japan. The depth-profile XPS measurements were performed at the Environmental Molecular Sciences Laboratory (EMSL), a national scientific user facility sponsored by the DOE Office of Biological and Environmental Research and located at Pacific Northwest National Laboratory. The operando XAS work at Advanced Light Source of Lawrence Berkeley National Laboratory was supported by the Director of the Office of Science, Office of Basic Energy Sciences, of DOE under contract no. DEAC02-05CH1123. We thank Dr. Sirine Fakra for her technical support at the beamline.

Author contributions

H.W. and J.-G.Z. conceived and designed the experiments. H.W. prepared electrolyte formulations, performed electrochemical measurements and fabricated cathode materials with

assistance from H.L.P., T.D., X.C. L, and D.P.L. X.F.F., G.X.R., Y.-S.L., J.F. and J.H.G. carried out operando XAS measurements and data analysis. Y.C and E. W. performed EPR measurements and data analysis. M.H.E. performed XPS measurements and data analysis with H.W. K. S. H. performed PFG-NMR measurements. H.W. and J.-G.Z. prepared this manuscript with inputs from Y.Y. S., H.L. P., and all other coauthors.

Competing interests

The authors declare no competing interests.

Corresponding authors

Correspondence to J.-G. Z.; Jiguang.zhang@pnnl.gov

Methods

Electrolyte preparation

The typical electrolyte formulation of 1 M LiTFSI_0.30 M Li nitrate ($LiNO_3$)_0.5 M Li_2S_4 in G2 was prepared as follows in an argon-filled glove box: $LiNO_3$ (99.99 %, Sigma-Aldrich) was first added to G2 (99.5%, Sigma-Aldrich) under stirring for 4 h at room temperature. Stoichiometric amounts of Li_2S (99.98%, Sigma-Aldrich) and S (99.5%, Alfa Aesar) were then added into this transparent solution and heated with vigorous stirring for 48 h at 80 °C. A homogeneous, dark-red solution was then obtained. LiTFSI was finally added to the as-obtained red solution with stirring for 4 h at 80 °C. The same method was applied to prepare E_G2_0.5 M Li_2S_4 and E_DOL/DME_saturated Li_2S_4, except added solvents. When the concentration of Li_2S_4 increased to 1.50 M, the concentration of $LiNO_3$ was correspondingly increased to 0.90 M. LiTFSI and $LiNO_3$ were dried for four days under vacuum at 120 °C, and the G2 was dried over activated 3Å molecular sieves in a glovebox prior to usage. Battery-grade DME (Gotion) and DOL (Gotion) were directly used as received to prepare the base electrolyte (E_DOL/DME) of 1 M LiTFSI_0.3 M $LiNO_3$ in DOL:DME (1:1 vol%).

Materials preparation

The ACFC_S_8 cathode was prepared by the adsorptive impregnation method described in our recent study[11]. CH700-20-type ACFC (pore volume: 0.878 $cm^3\ g^{-1}$; pore size: ≤ 2 nm; Brunauer-Emmet-Teller (BET) surface area: 1635 $m^2\ g^{-1}$; pore-clogged surface area: <10 $m^2\ g^{-1}$; thickness: ca. 500 μm) from Kuraray Co., Ltd, Japan, was employed as a model material, with a practical sulfur loading range of 6–8.5 mg cm^{-2}, to study electrolyte dependence of sulfur redox chemistry under lean electrolyte conditions. The ACFC_Li_2S_8 cathode was prepared by drop-casting a solution of 1 M Li_2S_8 in DME. The solution was prepared by dissolving 0.01 mol of Li (200 μm thick, MTI Corporation) and 0.04 mol of sulfur (99.5%, Alfa Aesar) in 5 mL of DME (battery grade, BASF) solution in a hermetically sealed glass vial at 80 °C. The prepared solution was stirred for about 18 h until a dark-red, homogeneous solution was obtained. Different

volumes (20–30 μL) of this mixture were dropped directly onto ACFC with a digital micropipette (Nichipet EX II 100, 10–100 μL, Nichiryo Co., Ltd.), and the DME solvent was allowed to evaporate at 120 °C under vacuum. The final amount of sulfur loading was controlled within the ACFC in the range of 4–6.5 mg cm^{-2}.

ECF was fabricated by electrospinning. Polyacrylonitrile (average MW 150,000, Sigma-Aldrich) and polymethylmethacrylate (MW = 120 000, Sigma-Aldrich) were dispersed at a 5:1 wt% ratio in anhydrous N,N-dimethylformamide (Sigma-Aldrich) and magnetically stirred for 20 h at 80 °C. Vacuum-dried silica nanoparticles (12 nm, LUDOX HS-30 colloidal silica, 30 wt % suspension in water, Sigma-Aldrich) were then added to this solution 2 wt %at a time. The as-prepared solution was fed through a syringe needle (BD 10 mL syringe, Luer-Lok tip) with the aid of an infusion syringe pump (78-0100C, Cole Parmer Instrument company, USA) at a constant flow rate of 1.20 mL h^{-1} and a DC voltage of 15 kV. The distance between the needle and the collector was 15 cm. The polymer composite membranes were stabilized in air at 250 °C for 1 h and subsequently carbonized at 700 °C for 3 h under Ar/H_2 flow (96:4, 100 cc min^{-1}). The membrane thickness ranged from 100 to 250 μm, and the mass loading was between 1.4 and 3.0 mg cm^{-2}. ECF-Li_2S_8 cathodes were prepared in the same way as ACFC_Li_2S_8 to assemble the Li-S cell. In the operando XAS measurement, SiO_2 was not added for the thin specimen of ECF_Li_2S_8.

Materials characterization

XPS measurements were performed with a Physical Electronics Quantera scanning X-ray microprobe. This system uses a focused, monochromatic, Al Kα X-ray (1486.7 eV) source for excitation and a spherical section analyzer. The instrument has a 32-element multichannel detection system. The X-ray beam is incident normal to the sample, and the photoelectron detector is at 45° off normal. High energy resolution spectra were collected using a pass energy of 69.0 eV with a step size of 0.125 eV. For the Ag 3d5/2 line, these conditions produced a full width at half maximum of 0.92 eV ± 0.05 eV. The binding energy scale was calibrated using the Cu 2p3/2 feature at 932.62 ± 0.05 eV and that of Au 4f7/2 at 83.96 ± 0.05 eV. All samples were rinsed with DME several times to remove residual electrolyte and then dried under vacuum for 20 min. To avoid side reactions or electrode contamination with ambient oxygen and moisture, electrodeposited Li was transported from the glovebox to the XPS and scanning electron microscope (SEM) instruments in a hermetically sealed container filled with Ar. The morphology of Li electrodeposited onto Cu was investigated using a Quanta focused-ion-beam SEM (FEI, Quanta 650 ESEM).

All EPR measurements were performed on a Bruker ELEXSYS E580 spectrometer at both 298 K and 125 K. All samples were prepared inside a glove box filled with nitrogen immediately before EPR experiments to minimize the influence of air and moisture. For liquid samples, a capillary with ID 0.8 mm and OD 1 mm was used to hold the solution in the EPR cavity with both ends sealed by Critoseal™ Leica Microsystems capillary tube sealant; the capillary was further placed inside a 4 mm EPR tube with the open end sealed inside a glove box. The typical settings for the spectra were microwave frequency = 9.32 GHz, sweep width = 1000 G, sweep time = 42 s, time constant = 40.96 ms, power = 20 mW, field modulation amplitude = 15 G. Absolute spin concentrations of the samples were determined by calibration

curves of the spin standard TEMPO (2,2,6,6-tetramethyl-1-piperidinyloxyl) with concentrations varying from 0.01 mM to 100 mM.

Lithium cation diffusion coefficient (D_{Li}) of the range of samples was determined by ^{7}Li pulsed field gradient (PFG) NMR measurement at Larmor frequency of 2π×232.98 rad MHz at 20 °C using a 14.1 T (600 MHz ^{1}H) NMR spectrometer (Agilent, USA) equipped with a 5 mm z-gradient probe (Doty Scientific, USA), which can generate a maximum gradient strength of ~31 T/m. The echo height, S(g), recorded as a function of gradient strength, g, was fitted with the Stejskal-Tanner equation, [45]

$$S(g) = S(0)e^{\text{¿¿}} \quad (1)$$

where S(g) and S(0) are the echo heights at the gradient strengths of g and 0, respectively, D is the diffusion coefficient, γ is ^{7}Li gyromagnetic ratio, Δ is the time interval between the two gradient pulses, i.e. diffusion delay, and δ is the gradient length. The PFG-echo profiles were obtained using the stimulated echo sequence employing the bipolar gradient pulses (Dbppste, a vender supplied sequence, Agilent, USA) as a function of gradient strength varied with 16 equal steps. The maximum gradient strength was chosen according to the echo height at the maximum gradient strength. The 90° pulse length, Δ and δ were 8 μs, 30 and 2 ms, respectively.

Micro-Raman measurements were performed using a 633 nm laser source, which was attenuated using a variable neutral density filter wheel (to 25 μW/μm^2), reflected off a dichroic beam splitter, and focused onto the sample using a 10X air objective. Our commercial Raman microscope is based on an inverted optical microscope (Nikon Ti-E) coupled to a Raman spectrometer (Horiba LabRAM HR). The backscattered light is collected through the same objective, transmitted through the beam splitter cube, and dispersed through a 600 l/mm grating. The effective resolution of the instrument in 3 cm^{-1} using this configuration.

Operando X-ray absorption spectroscopy measurements

Li-S battery cells of Li|Z_0.5 M Li_2S_4|ECF_Li_2S_8 were assembled in specially prepared CR2032 coin-cell cases. The cathode case was punched with a rectangular hole of 2 mm (horizontal) × 1 mm (vertical) at the center and tightly patched using 7 μm-thick Kapton tape, which has X-ray transmission of ~81% at 2470 eV). After assembly, no electrolyte leakage was observed. Li-S cells were tightly sealed in an aluminum foil envelope and then shipped to the Advanced Light Source (ALS), Lawrence Berkeley National Laboratory for the XAS measurements.

The *operando* XAS experiments were performed at Beamline 10.3.2 and 5.3.1 at the ALS. The X-ray beam size was 8 μm (horizontal) × 5 μm (vertical). The XAS spectra were collected in partial fluorescence-yield mode and calibrated using elemental sulfur spectra. All the S K-edge XAS spectra were collected under constant helium gas flow in a small chamber in front of the cell, and were acquired continuously during the discharging process.

Electrochemical measurements

The electrochemical characteristics of Li-S cells were investigated by PCGA, which is a common technique for characterization of electrochemical processes. In our case, PCGA was carried out by setting stepwise potential scans of 5 mV with a minimum current limit of 50 μA at

30 °C, using a Bio-Logic Instruments VSP potentiostat. The charge increment (δQ) was calculated by time integration of the current. Cyclic voltammetry measurements of Li-S cells were conducted at a scan rate of 0.2 mV s^{-1} in the range of 1.8–2.8 V at 30 °C.

Cathodes were punched into 1.267 cm^2 diameter disks and weighed to acquire the accurate sulfur loading for each piece. Added volume of electrolytes was determined by the sulfur loading, based on the E/S ratios, with a digital micropipette (Nichipet EX II 100, 10–100 μL, Nichiryo Co., Ltd.). Half-cells with 200 μm thick Li metal foil (MTI Corporation) as the anode and polyethylene (Asahi Kasai, Japan) as the separator were assembled using CR2032 coin cells in an MBraun LABmaster glove box with an Ar atmosphere (<1 ppm O_2 and <1 ppm H_2O). In the Li||Cu cell without the polyethylene separator, a thin polypropylene spacer r with a central hole was used to eliminate effects of a separator and crimping pressure on the morphology of Li electrodeposits. The galvanostatic discharge/charge cycles were tested using a LANHE battery tester in an incubator at 30 °C.

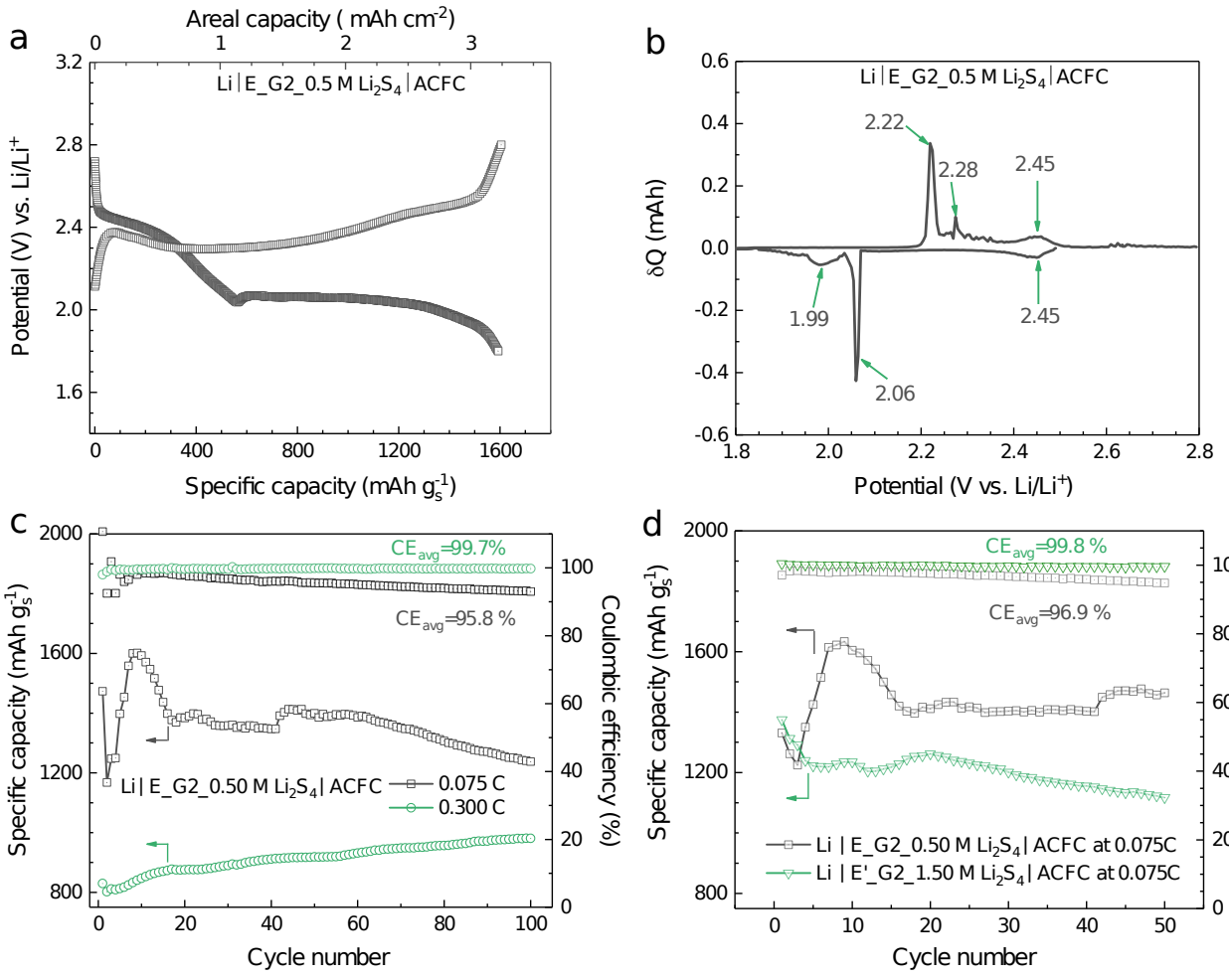

Figure 1 ┃ A new Li_2S_4-dictated pathway under lean electrolyte conditions. (a) A typical discharge/charge curve of Li ┃ E_G2_0.50 M Li_2S_4 ┃ ACFC cell after initial cycles at 0.075 C and 30 °C; (b) PCGA trace of Li┃E_G2_0.5 M Li_2S_4┃ACFC at 30 °C. Retention degree of Li_2S_4 is tuned in the bulk electrolytes using various discharge rates for E_G2_0.5 M Li_2S_4 (c) and the same low discharge rate of 0.075C in different concentrations of Li_2S_4 (d); Fig. 1a is the 9th cycle curve of the Li-S cell in Fig. 1c at 0.075C. Microporous activated carbon fiber cloth (ACFC) was used as a model material to study electrolyte dependence of the sulfur reduction pathway under lean electrolyte conditions. Different concentrations of Li_2S_4 were prepared in E_G2 (1 M LiTFSI_0.3 M $LiNO_3$ in G2) and E'_G2 (1 M LiTFSI_0.9 M $LiNO_3$ in G2).

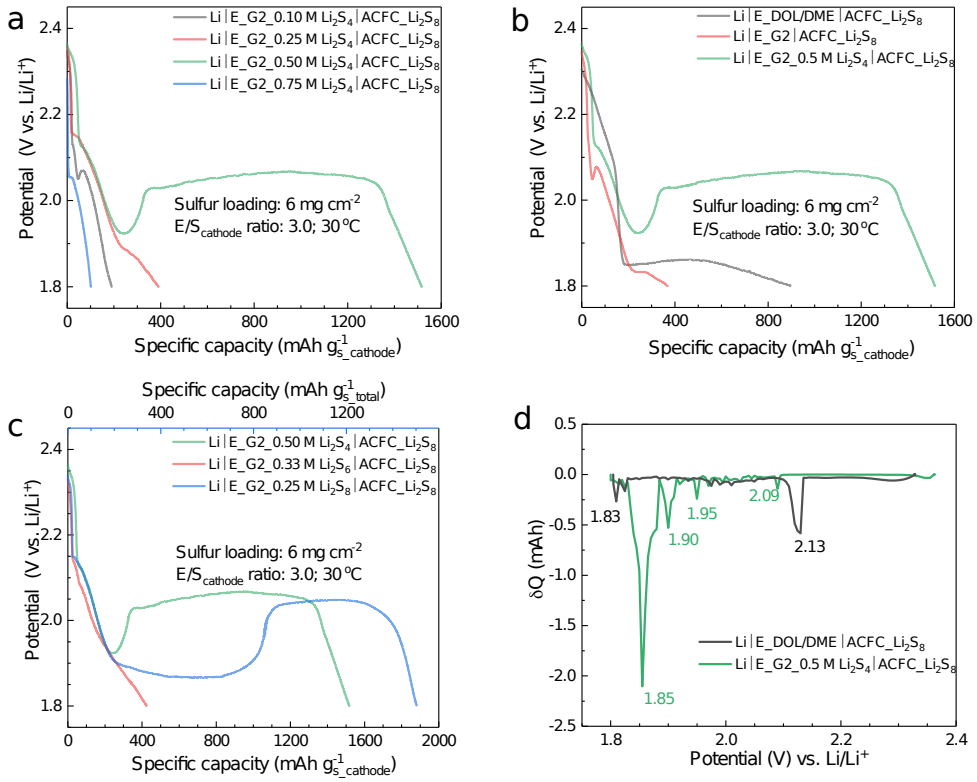

Figure 2 ❙ Li_2S_4-retention dependence on sulfur utilization. Electrolyte dependence of the typical discharge capacity for Li-S cells using ACFC-Li_2S_8 as the cathode with a sulfur loading of 6 mg cm^{-2} at an $E/S_{cathode}$ ratio of 3.0 mL_E $g_{S\_cathode}^{-1}$, 0.12 mA cm^{-2}, and 30 °C. The $g_{s\_cathode}$ represents the weight of sulfur in cathode. (a) using different concentrations of Li_2S_4 in Z; (b) using E_DOL/DME(1 M LiTFSI_0.3 M $LiNO_3$ in DOL/DME), E_G2, and E_G2_0.50 M Li_2S_4; (c) using different concentrations of LiPS with 2 M [S] in Z; (d) PCGA curves for the discharge of two Li-S cells with different electrolytes.

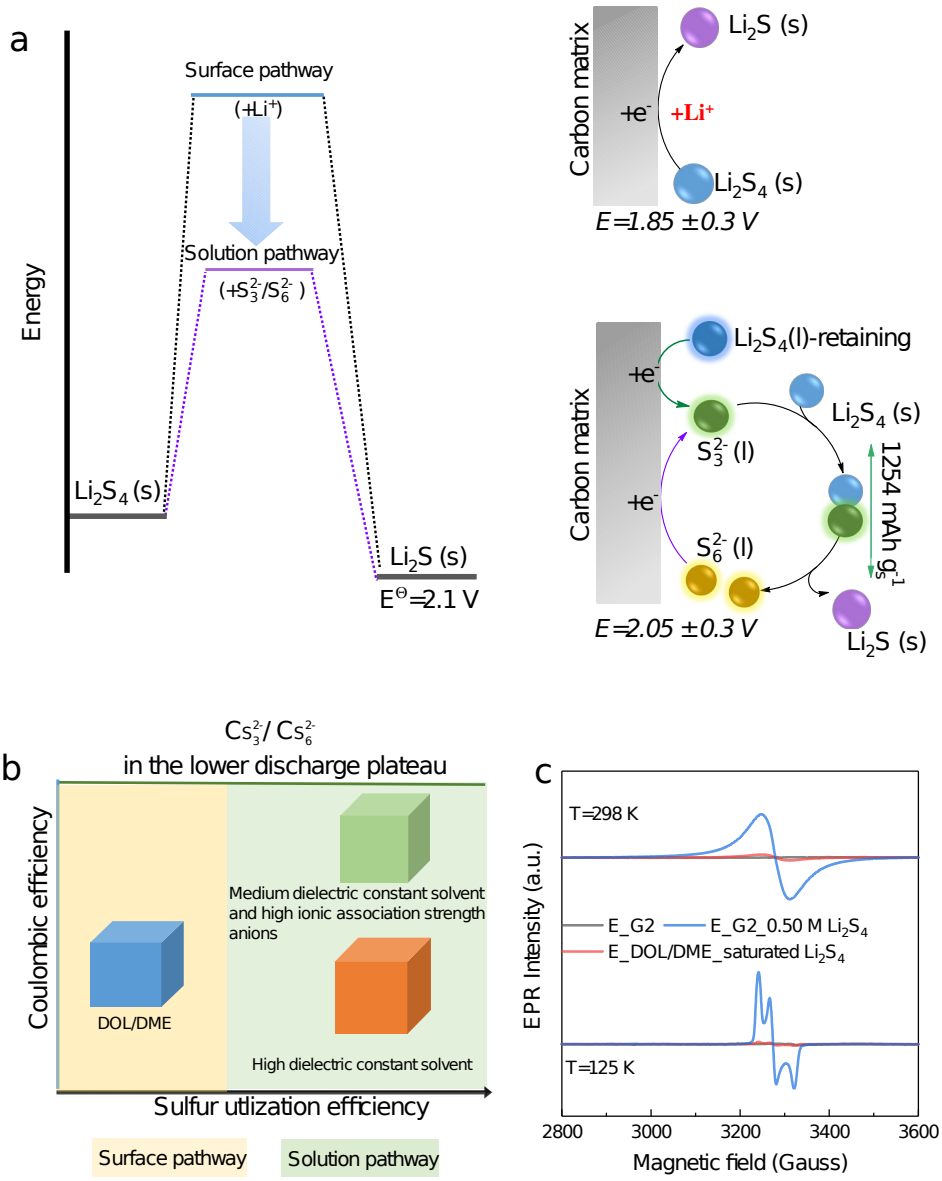

Figure 3 | Electrolyte dependence of sulfur discharge pathway. (a) Schematics of the effect of Li_2S_4-retaining solution pathway on the free-energy plot for Li_2S_4/Li_2S (left), and different pathways in the lower discharge plateau (right). S_6^{2-} is electrochemically reduced to S_3^{2-} at the carbon matrix surface, and then S_3^{2-} chemically reacts with solid Li_2S_4, producing solid Li_2S and itself being regenerated to S_6^{2-}. Initial S_3^{2-} comes from the reduction of S_4^{2-}-retaining in bulk electrolyte. As for the surface pathway, solid Li_2S_4 is electrochemically reduced with Li^+ to solid Li_2S with a higher overpotential at the carbon matrix surface; (b) Solvent and anion dependence of sulfur discharge pathway; (c) EPR spectra of E_G2, E_G2_0.5 M Li2S4 and E_DOL/DME_ saturated Li_2S_4 at 298 K (upper) and 125 K (lower).

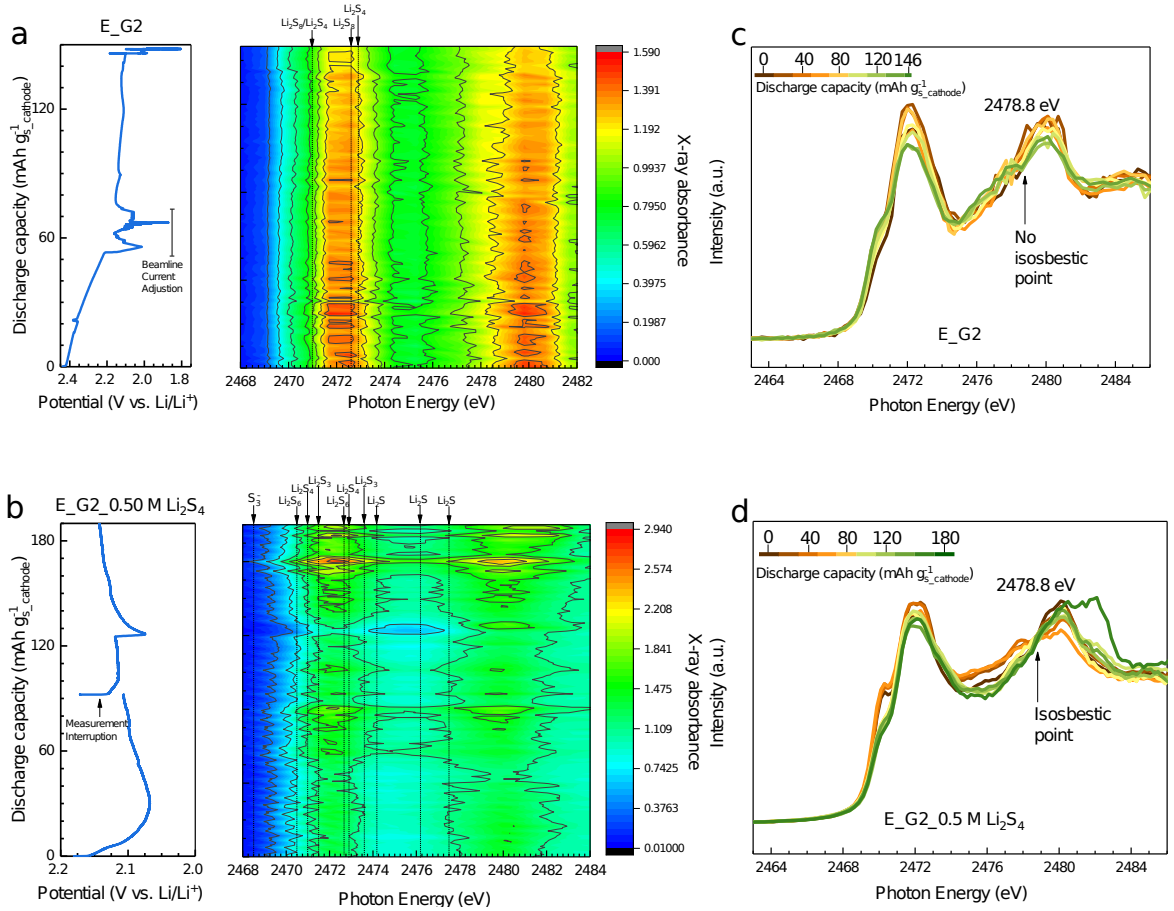

Figure 4 | Experimental corroboration of the Li_2S_4-retaining solution pathway. Normalized operando X-ray absorption spectroscopy (XAS) contours at the sulfur K-edge for (a) Li | E_G2 | ECF_Li_2S_8 (sulfur loading: 6 mg cm^{-2}; applied current density: 0.08 mA cm^{-2}) and (b) Li | E_G2_ Li_2S_4 | ECF_Li_2S_8 (sulfur loading: 4.3 mg cm^{-2}; applied current density: 0.04 mA cm^{-2}) upon initial discharge using electrospun carbon fiber (ECF) as the carbon matrix at an E/$S_{cathode}$ ratio of 3.0 mL_E $g_{S\_cathode}^{-1}$ and ambient temperature; the corresponding operando discharge curves of XAS Li-S cells are shown on the left. (c-d) the piling-up XAS spectra for the operando XAS cells of Li|E_G2|ECF_Li_2S_8 and Li|E_G2_ Li_2S_4|ECF_Li_2S_8 every 40 mAh $g_{S\_cathode}^{-1}$ until the end of discharging.

(a) (b)

Figure 5 | Application of the Li_2S_4-retaining solution pathway in a different carbon matrix-ECF. Voltage profiles vs. capacity (a) and cycling capacity retention and coulombic efficiency (b) of Li | E_G2_0.5 M Li_2S_4 | ECF_Li_2S_8 cell with a sulfur loading of 6.2 mg cm^{-2} at an E/$S_{cathode}$ ratio of 3.0 mL_E $g_{S\_cathode}^{-1}$, 0.20 mA cm^{-2}, and 30 °C in the range 1.80–2.45 V.

References

1. Larcher D, Tarascon JM. Towards greener and more sustainable batteries for electrical energy storage. *Nat Chem* **7**, 19 (2014).

2. Eroglu D, Zavadil KR, Gallagher KG. Critical Link between Materials Chemistry and Cell-Level Design for High Energy Density and Low Cost Lithium-Sulfur Transportation Battery. *J Electrochem Soc* **162**, A982-A990 (2015).

3. McCloskey BD. Attainable Gravimetric and Volumetric Energy Density of Li–S and Li Ion Battery Cells with Solid Separator-Protected Li Metal Anodes. *J Phys Chem Lett* **6**, 4581-4588 (2015).

4. Bruce PG, Freunberger SA, Hardwick LJ, Tarascon J-M. Li–O2 and Li–S batteries with high energy storage. *Nat Mater* **11**, 19 (2011).

5. Pan H*, et al.* Non-encapsulation approach for high-performance Li–S batteries through controlled nucleation and growth. *Nat Energy* **2**, 813-820 (2017).

6. Chen J*, et al.* Improving Lithium–Sulfur Battery Performance under Lean Electrolyte through Nanoscale Confinement in Soft Swellable Gels. *Nano Lett* **17**, 3061-3067 (2017).

7. Cheng X-B, Huang J-Q, Zhang Q. Review—Li Metal Anode in Working Lithium-Sulfur Batteries. *J Electrochem Soc* **165**, A6058-A6072 (2018).

8. Yan J, Liu X, Li B. Capacity Fade Analysis of Sulfur Cathodes in Lithium–Sulfur Batteries. *Adv Sci* **3**, 1600101 (2016).

9. Pang Q, Liang X, Kwok CY, Kulisch J, Nazar LF. A Comprehensive Approach toward Stable Lithium–Sulfur Batteries with High Volumetric Energy Density. *Adv Energy Mater* **7**, 1601630 (2017).

10. Pang Q, Shyamsunder A, Narayanan B, Kwok CY, Curtiss LA, Nazar LF. Tuning the electrolyte network structure to invoke quasi-solid state sulfur conversion and suppress lithium dendrite formation in Li–S batteries. *Nat Energy* **3**, 783-791 (2018).

11. Wang H*, et al.* Tailored Reaction Route by Micropore Confinement for Li–S Batteries Operating under Lean Electrolyte Conditions. *Adv Energy Mater* **8**, 1800590 (2018).

12. Shen C*, et al.* Understanding the role of lithium polysulfide solubility in limiting lithium-sulfur cell capacity. *Electrochim Acta* **248**, 90-97 (2017).

13. Li W*, et al.* The synergetic effect of lithium polysulfide and lithium nitrate to prevent lithium dendrite growth. *Nat Commun* **6**, 7436 (2015).

14. Dokko K*, et al.* Solvate Ionic Liquid Electrolyte for Li–S Batteries. *J Electrochem Soc* **160**, A1304-A1310 (2013).

15. Wang Q*, et al.* Direct Observation of Sulfur Radicals as Reaction Media in Lithium Sulfur Batteries. *J Electrochem Soc* **162**, A474-A478 (2015).

16. Aurbach D, Pollak E, Elazari R, Salitra G, Kelley CS, Affinito J. On the Surface Chemical Aspects of Very High Energy Density, Rechargeable Li–Sulfur Batteries. *J Electrochem Soc* **156**, A694-A702 (2009).

17. Xiong S, Xie K, Diao Y, Hong X. Characterization of the solid electrolyte interphase on lithium anode for preventing the shuttle mechanism in lithium-sulfur batteries. *J Power Sources* **246**, 840-845 (2014).

18. Barchasz C, Molton F, Duboc C, Leprêtre J-C, Patoux S, Alloin F. Lithium/Sulfur Cell Discharge Mechanism: An Original Approach for Intermediate Species Identification. *Anal Chem* **84**, 3973-3980 (2012).

19. Ren YX, Zhao TS, Liu M, Tan P, Zeng YK. Modeling of lithium-sulfur batteries incorporating the effect of Li2S precipitation. *J Power Sources* **336**, 115-125 (2016).

20. Cuisinier M, Cabelguen PE, Adams BD, Garsuch A, Balasubramanian M, Nazar LF. Unique behaviour of nonsolvents for polysulphides in lithium–sulphur batteries. *Energy Environ Sci* **7**, 2697-2705 (2014).

21. Lee C-W*, et al.* Directing the Lithium–Sulfur Reaction Pathway via Sparingly Solvating Electrolytes for High Energy Density Batteries. *ACS Cent Sci* **3**, 605-613 (2017).

22. Lowe MA, Gao J, Abruña HD. Mechanistic insights into operational lithium–sulfur batteries by in situ X-ray diffraction and absorption spectroscopy. *RSC Adv* **4**, 18347-18353 (2014).

23. Zhang G*, et al.* The Radical Pathway Based on a Lithium-Metal-Compatible High-Dielectric Electrolyte for Lithium–Sulfur Batteries. *Angew Chem, Int Ed* **57**, 16732-16736 (2018).

24. Lodovico L, Varzi A, Passerini S. Radical Decomposition of Ether-Based Electrolytes for Li-S Batteries. *J Electrochem Soc* **164**, A1812-A1819 (2017).

25. Yim T*, et al.* Effect of chemical reactivity of polysulfide toward carbonate-based electrolyte on the electrochemical performance of Li–S batteries. *Electrochim Acta* **107**, 454-460 (2013).

26. Zou Q, Lu Y-C. Solvent-Dictated Lithium Sulfur Redox Reactions: An Operando UV–vis Spectroscopic Study. *J Phys Chem Lett* **7**, 1518-1525 (2016).

27. Cuisinier M, Hart C, Balasubramanian M, Garsuch A, Nazar LF. Radical or Not Radical: Revisiting Lithium–Sulfur Electrochemistry in Nonaqueous Electrolytes. *Adv Energy Mater* **5**, 1401801 (2015).

28. Pan H*, et al.* On the Way Toward Understanding Solution Chemistry of Lithium Polysulfides for High Energy Li–S Redox Flow Batteries. *Adv Energy Mater* **5**, 1500113 (2015).

29. Ueno K*, et al.* Anionic Effects on Solvate Ionic Liquid Electrolytes in Rechargeable Lithium–Sulfur Batteries. *J Phys Chem C* **117**, 20509-20516 (2013).

30. Fan FY, Chiang Y-M. Electrodeposition Kinetics in Li-S Batteries: Effects of Low Electrolyte/Sulfur Ratios and Deposition Surface Composition. *J Electrochem Soc* **164**, A917-A922 (2017).

31. Elazari R, Salitra G, Garsuch A, Panchenko A, Aurbach D. Sulfur-Impregnated Activated Carbon Fiber Cloth as a Binder-Free Cathode for Rechargeable Li-S Batteries. *Adv Mater* **23**, 5641-5644 (2011).

32. Markevich E, Salitra G, Rosenman A, Talyosef Y, Chesneau F, Aurbach D. The effect of a solid electrolyte interphase on the mechanism of operation of lithium–sulfur batteries. *J Mater Chem A* **3**, 19873-19883 (2015).

33. Xu R, Lu J, Amine K. Progress in Mechanistic Understanding and Characterization Techniques of Li-S Batteries. *Adv Energy Mater* **5**, 1500408-n/a (2015).

34. Hagen M*, et al.* In-Situ Raman Investigation of Polysulfide Formation in Li-S Cells. *J Electrochem Soc* **160**, A1205-A1214 (2013).

35. Pascal TA*, et al.* X-ray Absorption Spectra of Dissolved Polysulfides in Lithium–Sulfur Batteries from First-Principles. *J Phys Chem Lett* **5**, 1547-1551 (2014).

36. Wujcik KH, Wang DR, Pascal TA, Prendergast D, Balsara NP. In Situ X-ray Absorption Spectroscopy Studies of Discharge Reactions in a Thick Cathode of a Lithium Sulfur Battery. *J Electrochem Soc* **164**, A18-A27 (2017).

37. Zhang S. Improved Cyclability of Liquid Electrolyte Lithium/Sulfur Batteries by Optimizing Electrolyte/Sulfur Ratio. *Energies* **5**, 5190 (2012).

38. Zhang L, Sun D, Feng J, Cairns EJ, Guo J. Revealing the Electrochemical Charging Mechanism of Nanosized Li2S by in Situ and Operando X-ray Absorption Spectroscopy. *Nano Lett* **17**, 5084-5091 (2017).

39. Liang X, Hart C, Pang Q, Garsuch A, Weiss T, Nazar LF. A highly efficient polysulfide mediator for lithium–sulfur batteries. *Nat Commun* **6**, 5682 (2015).

40. Yang X*, et al.* Promoting the Transformation of Li2S2 to Li2S: Significantly Increasing Utilization of Active Materials for High-Sulfur-Loading Li–S Batteries. *Adv Mater* **31**, 1901220 (2019).

41. Pascal TA, Wujcik KH, Wang DR, Balsara NP, Prendergast D. Thermodynamic origins of the solvent-dependent stability of lithium polysulfides from first principles. *Phys Chem Chem Phys* **19**, 1441-1448 (2017).

42. Su Y-S, Fu Y, Cochell T, Manthiram A. A strategic approach to recharging lithium-sulphur batteries for long cycle life. *Nat Commun* **4**, 2985 (2013).

43. Li M*, et al.* A Lithium–Sulfur Battery using a 2D Current Collector Architecture with a Large-Sized Sulfur Host Operated under High Areal Loading and Low E/S Ratio. *Adv Mater* **30**, 1804271 (2018).

44. Xue W, *et al.* Intercalation-conversion hybrid cathodes enabling Li–S full-cell architectures with jointly superior gravimetric and volumetric energy densities. *Nat Energy*, (2019).

45. Johnson Jr CS. Diffusion ordered nuclear magnetic resonance spectroscopy: principles and applications. *Progress in Nuclear Magnetic Resonance Spectroscopy* **34**, 203-256 (1999).